


Triaxiality-induced monopole-quadrupole-hexadecupole coupling in the isoscalar giant resonances of ^{86}Ge

Xuwei Sun *State Key Laboratory of Nuclear Physics and Technology, School of Physics, Peking University, Beijing 100871, China*Jie Meng **State Key Laboratory of Nuclear Physics and Technology, School of Physics, Peking University, Beijing 100871, China and Yukawa Institute for Theoretical Physics, Kyoto University, Kyoto 606-8502, Japan*

(Received 8 June 2022; accepted 18 August 2022; published 30 August 2022)

The isoscalar giant resonances for ^{86}Ge are studied by the quasiparticle finite amplitude method based on the covariant density functional theory. In addition to the well-known monopole-quadrupole coupling that splits the isoscalar giant monopole resonance in axially deformed nuclei, a monopole-quadrupole-hexadecupole coupling is identified in the neutron-rich triaxially deformed nucleus ^{86}Ge , leading to the emergence of a distinct resonance peak at the low energy side of the isoscalar monopole strength function. The transition density of the triaxiality-induced resonance peak shows a strong interplay among monopole, quadrupole, and hexadecupole vibrations. The resonance peak responds to monopole, quadrupole, and hexadecupole perturbations simultaneously, which could be regarded as a fingerprint of the triaxiality in ^{86}Ge .

DOI: [10.1103/PhysRevC.106.024334](https://doi.org/10.1103/PhysRevC.106.024334)

I. INTRODUCTION

Giant resonances (GRs) [1] are small amplitude collective vibrations of a nucleus which are related to nuclear bulk properties, e.g., via certain sum rules [2], and provide valuable information on nuclear structure such as incompressibility [3–7], symmetry energy [8–10], and neutron skin thickness [11–14].

The effect of axial deformation describing prolate or oblate spheroid shapes on GRs has been extensively discussed [15–17]. In particular, shortly after the discovery of the isoscalar giant monopole resonance (ISGMR) [18], it was reported that the ISGMRs for well-deformed nuclei split into two branches [19]. The splitting is caused by the coupling between ISGMR and isoscalar giant quadrupole resonance (ISGQR) with $K = 0$, namely, the monopole-quadrupole coupling ($E0$ - $E2$ coupling). Experimental evidence of the $E0$ - $E2$ coupling is found for ^{150}Nd [20], ^{154}Sm [21], ^{181}Ta [22], ^{238}U [23], etc. Explanations and predictions of the $E0$ - $E2$ coupling are made by macroscopic calculations through cranking model [24], variational procedure [25], fluid dynamical description [26], and random phase approximation calculations [27–29].

Apart from elongating or compressing along the symmetry axis of the intrinsic frame, a nucleus can be further squeezed perpendicularly to its symmetry axis, and has a triaxially deformed shape. Triaxial deformation is thought to be the key ingredient for a lot of interesting phenomena such as nuclear chirality [30,31] and wobbling [32]. Triaxiality will also affect

GRs in a significant way. For example, a recent work suggests that triaxiality sheds light upon the softening of ISGMRs for cadmium isotopes [33].

The microscopic random phase approximation (RPA) method [34] is widely used in studying nuclear collective vibrations. Combined with modern nuclear energy density functionals [35–37], the RPA method is able to give successful descriptions of nuclear giant resonances [38–40]. For deformed and superfluid nuclei, the full configuration space of RPA is huge, and solving RPA equations is extremely challenging if no artificial truncation is applied. The finite amplitude method (FAM) [41] provides a numerical feasible way to solve large scale RPA problems. In spherical and axially deformed cases, FAM has been implemented on both relativistic [27,42–45] and nonrelativistic [46–49] density functionals. In the triaxially deformed case, FAM is so far implemented for Skyrme density functional theory in the three-dimensional Cartesian coordinate space [50], as well as for covariant density functional theory (CDFT) in a triaxially deformed harmonic oscillator basis [33], making it possible to study triaxial deformation effects on GRs in a microscopic and self-consistent way.

Though the $E0$ - $E2$ coupling in axially deformed nuclei has been well understood, the situation in triaxially deformed nuclei demands further study. It is also interesting to search for possible distinctive resonance structures caused by the triaxiality. The paper is devoted to investigating the impact of triaxiality on the GRs by the triaxially deformed quasiparticle finite amplitude method (QFAM) on CDFT [33]. The outline of the paper is as follows. Section II presents the formalism of CDFT and QFAM. In Sec. III, the triaxiality effects on the isoscalar giant resonances for the triaxially deformed nucleus

*mengj@pku.edu.cn

^{86}Ge will be analyzed. Conclusions and remarks will be given in Sec. IV.

II. FORMALISM

In this section, the nuclear CDFT [36] with effective meson-exchange interaction, and the implementation of the QFAM will be briefly introduced.

In CDFT, the effective nuclear forces are mediated by the scalar meson σ , the vector meson ω_μ , the vector-isovector meson $\vec{\rho}_\mu$, and the photon A_μ . The interacting part of the Lagrangian density is

$$\mathcal{L}_{\text{int}} = - \sum_m g_m \bar{\psi} \Gamma_m \cdot \phi_m \psi, \quad (1)$$

where $\Gamma_m = \{1, \gamma^\mu, \vec{\tau}\gamma^\mu, (1 - \tau_3)\gamma^\mu/2\}$ is the coupling vertex between the nucleon ψ and the meson (photon) $\phi_m = \{\sigma, \omega_\mu, \vec{\rho}_\mu, A_\mu\}$ with the coupling strength g_m .

The state of a nuclear system $|\Phi\rangle$ can be uniquely expressed by the density operator $\hat{\rho}$. The matrix element of density operator $\hat{\rho}$ in a single particle basis has the form [34]

$$\rho_{pq} = \langle \Phi | c_q^\dagger c_p | \Phi \rangle. \quad (2)$$

The Hamiltonian density can be transformed from the Lagrangian density, its expectation value in the state $|\Phi\rangle$ is the following density functional:

$$\begin{aligned} \epsilon[\hat{\rho}, \phi] &= \text{Tr}[-i\alpha\nabla + \beta m]\hat{\rho} + \sum_m \text{Tr}[\beta g_m \Gamma_m \phi_m \hat{\rho}] \\ &\pm \sum_m \frac{1}{2} \int d^3r [(\partial_\mu \phi_m)^2 + m_m^2 \phi_m^2]. \end{aligned} \quad (3)$$

The equation of motion of the density operator and meson (photon) field can be derived from the time-dependent variation principle,

$$\delta \int_{t_1}^{t_2} dt \{ \langle \Phi | i\partial_t | \Phi \rangle - \epsilon[\hat{\rho}, \phi] \} = 0, \quad (4)$$

and reads.

$$\begin{aligned} i\partial_t \hat{\rho} &= [\hat{h}, \hat{\rho}], \\ (\partial^v \partial_v + m_m^2) \phi_m &= \mp \text{Tr}[\beta g_m \Gamma_m \hat{\rho}]. \end{aligned} \quad (5)$$

The singleparticle Hamiltonian \hat{h} is

$$\hat{h}[\hat{\rho}, \phi] \equiv \frac{\delta \epsilon[\hat{\rho}, \phi]}{\delta \hat{\rho}} = -\alpha(i\nabla + \mathbf{V}) + V_0 + \beta(m + S), \quad (6)$$

with the scalar potential S and the vector potential $V_\mu \equiv (V_0, \mathbf{V})$ consisting of the meson and photon fields,

$$\begin{aligned} S &= g_\sigma \sigma, \\ V_\mu &= g_\omega \omega_\mu + g_\rho \vec{\tau} \cdot \vec{\rho}_\mu + e \frac{1 - \tau_3}{2} A_\mu + \Sigma_\mu^R. \end{aligned} \quad (7)$$

The rearrangement term Σ_μ^R appears when the coupling strength g_m is density dependent [51]. For even-even nuclei, the spatial components of the vector potential vanish due to the time-reversal symmetry.

With a pairing interaction V^{pp} , the matrix elements of the pairing tensor $\hat{\kappa}$ is

$$\kappa_{pq} = \langle \Phi | c_q c_p | \Phi \rangle, \quad (8)$$

from which the pairing energy is evaluated,

$$\epsilon[\hat{\kappa}] = \frac{1}{4} \text{Tr}[\hat{\kappa}^* V^{pp} \hat{\kappa}], \quad (9)$$

and a pairing potential $\hat{\Delta}$ can be defined:

$$\hat{\Delta} \equiv \frac{\delta \epsilon[\hat{\kappa}]}{\delta \hat{\kappa}}. \quad (10)$$

The density and the pairing tensor can be expressed in a compact form via the generalized density [52]

$$\hat{\mathcal{R}} = \begin{pmatrix} \hat{\rho} & \hat{\kappa} \\ -\hat{\kappa}^* & 1 - \hat{\rho}^* \end{pmatrix}, \quad (11)$$

and the generalized Hamiltonian is obtained accordingly:

$$\hat{\mathcal{H}} = \frac{\delta(\epsilon[\hat{\rho}, \phi] + \epsilon[\hat{\kappa}])}{\delta \hat{\mathcal{R}}} = \begin{pmatrix} \hat{h} & \hat{\Delta} \\ -\hat{\Delta}^* & -\hat{h}^* \end{pmatrix}. \quad (12)$$

Diagonalizing the generalized Hamiltonian gives the relativistic Hartree-Bogoliubov (RHB) equation [34]

$$\begin{pmatrix} \hat{h} - \lambda & \hat{\Delta} \\ -\hat{\Delta}^* & -\hat{h}^* + \lambda \end{pmatrix} \begin{pmatrix} U_\mu \\ V_\mu \end{pmatrix} = E_\mu \begin{pmatrix} U_\mu \\ V_\mu \end{pmatrix}, \quad (13)$$

where a chemical potential λ is introduced to account for particle number conservation [34]. E_μ is the quasiparticle energy. The RHB equation is solved by an expansion of the quasiparticle spinor U_μ, V_μ on a triaxial harmonic oscillator basis [53], which is the product of three one-dimensional harmonic oscillator wavefunction and a spin factor,

$$\phi_i(x, y, z) = \varphi_{n_x}(x) \varphi_{n_y}(y) \varphi_{n_z}(z) \chi_{m_s}, \quad (14)$$

labeled by a set of quantum numbers $i \equiv \{n_x, n_y, n_z; m_s\}$.

If a nucleus is perturbed by a weak external field $\mathcal{F}(t)$ with the frequency ω , its density $\mathcal{R}(t)$ and Hamiltonian $\mathcal{H}(t)$ vibrates slightly around the equilibrium \mathcal{R}_0 and \mathcal{H}_0 . The following small-amplitude approximation is valid:

$$\begin{aligned} \mathcal{R}(t) &= \mathcal{R}_0 + \delta \mathcal{R}(\omega) e^{-i\omega t} + \text{H.c.}, \\ \mathcal{H}(t) &= \mathcal{H}_0 + \delta \mathcal{H}(\omega) e^{-i\omega t} + \text{H.c.} \end{aligned} \quad (15)$$

From the equation of motion $i\dot{\mathcal{R}}(t) = [\mathcal{H}(t) + \mathcal{F}(t), \mathcal{R}(t)]$, the linear response equation can be obtained:

$$\begin{aligned} (E_\mu + E_\nu - \omega) X_{\mu\nu}(\omega) + \delta H_{\mu\nu}^{20}(\omega) &= -F_{\mu\nu}^{20}, \\ (E_\mu + E_\nu + \omega) Y_{\mu\nu}(\omega) + \delta H_{\mu\nu}^{02}(\omega) &= -F_{\mu\nu}^{02}. \end{aligned} \quad (16)$$

The quasiparticle energy E_μ, E_ν , and the matrix element of external field $F_{\mu\nu}^{20}, F_{\mu\nu}^{02}$ are independent of the excitation energy ω . The induced Hamiltonian $\delta H(\omega)$ is a functional of the transition amplitudes $X(\omega)$ and $Y(\omega)$; they are calculated via the following finite amplitude method.

The matrix elements of the induced Hamiltonian $\delta H(\omega)$ in quasiparticle basis can be calculated from the variation of the single-particle Hamiltonian $\delta h(\omega)$ and the variation of the

pairing potential $\delta\Delta(\omega)$, $\delta\Delta^*(\omega)$,

$$\begin{aligned}\delta H_{\mu\nu}^{20}(\omega) &= [U^\dagger \delta h(\omega) V^* - V^\dagger \delta h^T(\omega) U^* \\ &\quad - V^\dagger \delta\Delta^*(\omega) V^* + U^\dagger \delta\Delta(\omega) U^*]_{\mu\nu}, \\ \delta H_{\mu\nu}^{02}(\omega) &= [U^T \delta h^T(\omega) V - V^T \delta h(\omega) U \\ &\quad - V^T \delta\Delta(\omega) V + U^T \delta\Delta^*(\omega) U]_{\mu\nu}.\end{aligned}\quad (17)$$

The transition amplitudes $X(\omega)$ and $Y(\omega)$ are used to get the variation of the single-particle density, $\delta\rho(\omega)$, and the variations of the pairing tensor, $\delta\kappa(\omega)$ and $\delta\kappa^*(\omega)$, whose matrix elements in the harmonic oscillator basis read

$$\begin{aligned}\delta\rho_{ij}(\omega) &= [UX(\omega)V^T + V^*Y(\omega)U^\dagger]_{ij}, \\ \delta\kappa_{ij}(\omega) &= [UX(\omega)U^T + V^*Y(\omega)V^\dagger]_{ij}, \\ \delta\kappa_{ij}^*(\omega) &= -[VX(\omega)V^T - U^*Y(\omega)U^\dagger]_{ij}.\end{aligned}\quad (18)$$

The variations $\delta h(\omega)$ [$\delta\Delta(\omega)$ and $\delta\Delta^*(\omega)$] are calculated from the difference between the single-particle Hamiltonian [the pairing field] at the perturbed density and at the equilibrium ρ_0 [κ_0 and κ_0^*],

$$\begin{aligned}\delta h(\omega) &= \frac{1}{\eta} \{h[\rho_0 + \eta\delta\rho(\omega)] - h[\rho_0]\}, \\ \delta\Delta(\omega) &= \frac{1}{\eta} \{\Delta[\kappa_0 + \eta\delta\kappa(\omega)] - \Delta[\kappa_0]\}, \\ \delta\Delta^*(\omega) &= \frac{1}{\eta} \{\Delta^*[\kappa_0^* + \eta\delta\kappa^*(\omega)] - \Delta^*[\kappa_0^*]\},\end{aligned}\quad (19)$$

with a small real parameter $\eta = 10^{-6}$.

Once the connection from the transition amplitude to the induced Hamiltonian is established, Eq. (16) can be solved iteratively. The converged transition amplitudes $X_{\mu\nu}(\omega)$ and $Y_{\mu\nu}(\omega)$ are used to calculate the strength function,

$$S_F(\hat{F}, \omega) = -\frac{1}{\pi} \text{Im} \sum_{\mu\nu} \{F_{\mu\nu}^{20*} X_{\mu\nu}(\omega) + F_{\mu\nu}^{02*} Y_{\mu\nu}(\omega)\}.\quad (20)$$

In this work, the functional we used is DD-ME2 [51], and the pairing interaction is a separable pairing force [54]. Due to the numerical feasibility of QFAM, there is no artificial truncation being applied on the two quasiparticle pairs. The calculations are performed on a harmonic oscillator basis with 12 shells, and the amount of two-quasiparticle pairs involved in the QFAM calculation is $N_{2qp} = 2086560$. In fully self-consistent QFAM calculations, the symmetry broken in the ground state will be restored, which automatically generates a zero-energy Nambu-Goldstone boson. For instance, the particle number conservation broken in the RHB level is recovered in the QFAM calculation. Therefore, a spurious state with a vanishing energy appears in the strength function for the particle number operator \hat{N} , as illustrated in Fig. 1.

III. RESULTS AND DISCUSSIONS

The potential-energy surface (PES) with the deformation parameter (β, γ) [53] is illustrated in Figs. 2(a)–2(c) for ^{64}Ge , ^{74}Ge , and ^{86}Ge , respectively. Though all of these nuclei are triaxially deformed, their monopole strength functions response

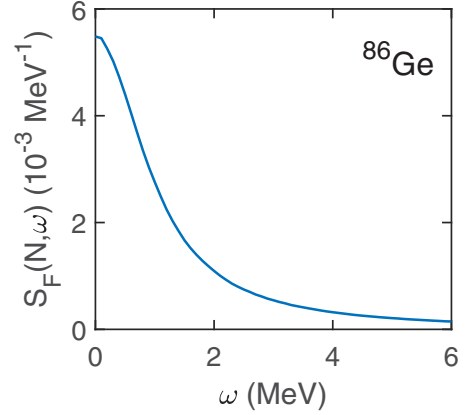


FIG. 1. Strength function for the particle number operator \hat{N} . The spurious state centers at zero energy, since the particle-number conservation has been restored by the QFAM calculation.

to the triaxiality differently, as shown in Figs. 2(d)–2(f). For ^{64}Ge which has a prominent triaxial minimal in the PES, the monopole strength function is fragmented by the triaxiality. For ^{74}Ge whose PES is γ -soft, the monopole strength function shifts to low energy side slightly when the triaxiality is considered. For ^{86}Ge , the effect of triaxiality on monopole strength function seems extremely interesting as it induces a distinct low-lying resonance peak. Since monopole resonance involves $2\hbar\omega$ particle-hole transitions [1] whose energies are large for stable nuclei, the low-lying monopole resonances could be hardly expected for nuclei close to the stability line. In contrast, in nuclei far from the stability line the low-lying monopole resonance may appear, because in these nuclei nucleons near Fermi surface could have small-energy $2\hbar\omega$ transitions. Therefore, ^{86}Ge could provide us the chance to learn how triaxiality impacts the low-lying monopole resonance. In the following, the details will be analyzed by the state-of-the-art triaxial QFAM.

The PES of ^{86}Ge shows a minimum at $\beta = 0.234$ and $\gamma = 20.9^\circ$; namely, the ground state of ^{86}Ge is triaxially deformed. In the axial deformation calculation, there are a prolate minimum at $\beta = 0.209$ with $E = 0.62$ MeV and an oblate minimum at $\beta = 0.191$ with $E = 1.70$ MeV; the ground state is prolate deformed. Compared to the axially deformed case, the existence of triaxial deformation makes ^{86}Ge more elongated in the z direction.

The lifetime of the nucleus ^{86}Ge is about 226 ms [55], which might make study of its giant resonances possible with the rapid development of radioactive beam facilities. In order to look for possible vibration properties peculiar to triaxiality, both triaxial QFAM calculation and axial QFAM calculations are performed to study the giant resonances for ^{86}Ge , with the density functional DD-ME2 [51] and the separable pairing force [54]. In Fig. 3, the strength functions of ISGMR, ISGQR with $K = 0$, and isoscalar giant hexadecupole resonance (ISGHR) with $K = 0$ for ^{86}Ge are presented. The strength functions are obtained by perturbing the nucleus with monopole, quadrupole, and hexadecupole vibrations, using the corresponding external field operators $\hat{Q}_{00} = r^2$, $\hat{Q}_{20} = r^2 Y_{20}$, and $\hat{Q}_{40} = r^4 Y_{40}$. A smearing width of 2 MeV is used to

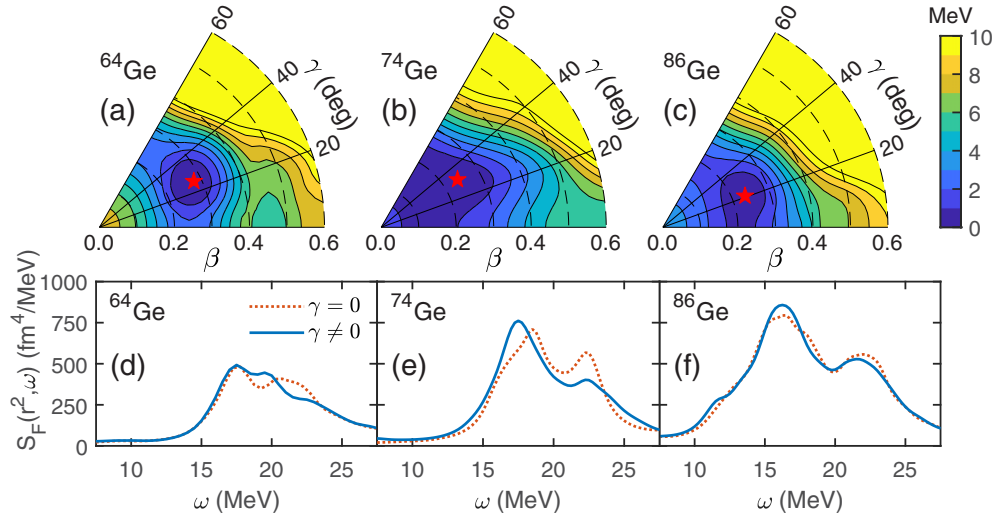


FIG. 2. Potential-energy surfaces [(a)–(c)] and monopole strength functions [(d)–(f)] of $^{64,74,86}\text{Ge}$ calculated by CDFT with DD-ME2 and a separable pairing force. The PES is illustrated by contours spacing 1 MeV, with a red pentagram denoting the minimal. The monopole strength functions with (solid blue line) and without (dotted red line) the effect of triaxiality are smeared with $\Gamma = 2$ MeV.

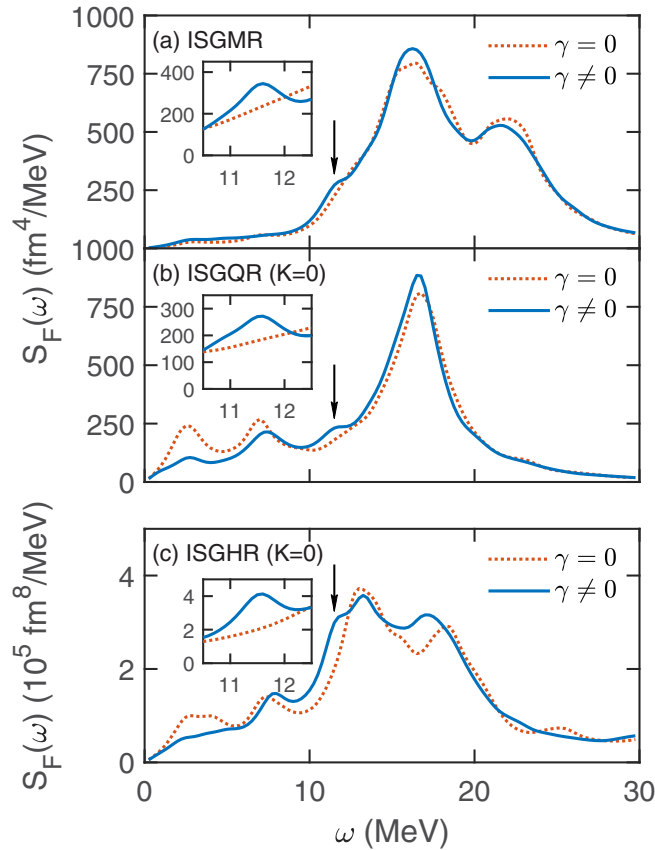


FIG. 3. (a) ISGMR, (b) ISGQR with $K = 0$, and (c) ISGHR with $K = 0$ for ^{86}Ge with (solid blue line) and without (dotted red line) the effect of triaxial deformation. The arrow in each panel denotes the peak due to the triaxial deformation, which is also highlighted in the corresponding inset with a smearing width $\Gamma = 1$ MeV.

take into account the spreading effects [33]. The results for the triaxially deformed case and for the axially deformed case are drawn with solid blue lines and dotted red lines, respectively.

For the ISGMR, two branches of resonances can be identified when axial deformation is considered. The main peak of ISGMR locates higher and a pronounced peak appears at the lower excitation energy. The monopole vibration has no directional projection, so that the ISGMR cannot split itself. The reason for the splitting is the monopole-quadrupole coupling between the ISGMR and the ISGQR with $K = 0$ [27–29]. As can be identified in panel (a) and (b), the lower branch of ISGMR locates at the same position as the ISGQR with $K = 0$. When the triaxial deformation is considered, the locations of the aforementioned peaks remain nearly unchanged, but the strength is slightly promoted for the lower one and reduced for the higher one. Because in the triaxially deformed case ^{86}Ge is more elongated in the z direction, the $E0$ - $E2$ coupling is stronger and pumps more strength to the lower peak.

Since the lower branch of the ISGMR is aroused by the $E0$ - $E2$ coupling, it should contain considerable contributions from quadrupole vibrations. To see this, in Fig. 4, the transition density, defined via

$$\delta\rho(\omega, x, y, z) = \sum_{i,j} \phi_i^\dagger(x, y, z) \delta\rho_{ij}(\omega) \phi_j(x, y, z), \quad (21)$$

for the lower branch of ISGMR near 16.5 MeV is presented, with the distributions on the $z = 0$, $y = 0$, and $x = 0$ planes in panels (a)–(c). The transition density for the ISGQR with $K = 0$ are also presented in panels (d)–(f) for comparison, from which it is clear that the vibration along the z axis is out of phase with the vibration perpendicular to the z axis. The transition density for the ISGMR has a similar feature, but shows a strong mixture from the monopole vibration in the interior of the nucleus. Therefore, triaxiality seems to introduce no substantial difference to the main peaks of ISGMR, and the

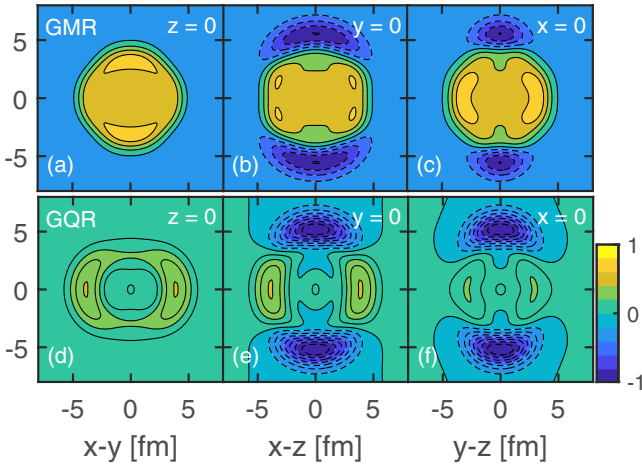


FIG. 4. Normalized transition densities at 16.5 MeV in ^{86}Ge for the resonance peaks of ISGMR [(a)–(c)], and the ISGQR with $K = 0$ [(d)–(f)]. Contours with positive (negative) values are drawn with solid (dashed) lines.

monopole-quadrupole coupling is still valid for the triaxially deformed nucleus ^{86}Ge .

The most notable observation about the ISGMR in the triaxially deformed case is that a small peak emerges near $\omega \approx 11.5$ MeV in the strength function, as denoted by the arrow in Fig. 3(a). The same resonance peak can also be found in the strength function of ISGQR presented in Fig. 3(b). As for the ISGHR in Fig. 3(c), it appears as a shoulder at the low energy side of the main peak and enhances the strength function between 10 to 12 MeV. Indeed, triaxiality also impacts the low-energy strengths for ISGQR and ISGHR, e.g., quenching the strength functions around 2.5 and 7 MeV. However, as this work is devoted to investigating the effect peculiar to triaxiality, we would like to focus on the resonance peak at around 11.5 MeV, which will vanish if the triaxiality is not considered. In the insets of Fig. 3, a small smearing width $\Gamma = 1$ MeV is used to show the details of the strength functions, and the peak near 11.5 MeV is highlighted. This triaxiality-induced resonance peak is discernible for ISGMR, and is pronounced for ISGQR and ISGHR. The fraction of the energy weighted moment exhausted by the triaxiality-induced resonance peak, calculated by accumulating the energy weighted strength function from 10 to 12 MeV for the triaxially deformed case and then subtracting that for the axially deformed case, varies from 0.55% for ISGMR to 1.02% for ISGQR to 2.58% for ISGHR.

In a deformed nucleus, the monopole vibration may couple to the $K = 0$ component of other even- J vibrations. Since the resonance peak at 11.5 MeV responds to the monopole, the quadrupole, as well as the hexadecupole perturbations simultaneously, it should contain a mixture from the monopole, quadrupole, and hexadecupole vibrations. In close analogy to the ISGMR splitting that manifests the monopole-quadrupole ($E0$ - $E2$) coupling, the triaxiality-induced resonance peak might be an indicator of the coupling of the ISGMR and the ISGQR as well as the ISGHR with $K = 0$, i.e., the monopole-quadrupole-hexadecupole ($E0$ - $E2$ - $E4$) coupling. To verify

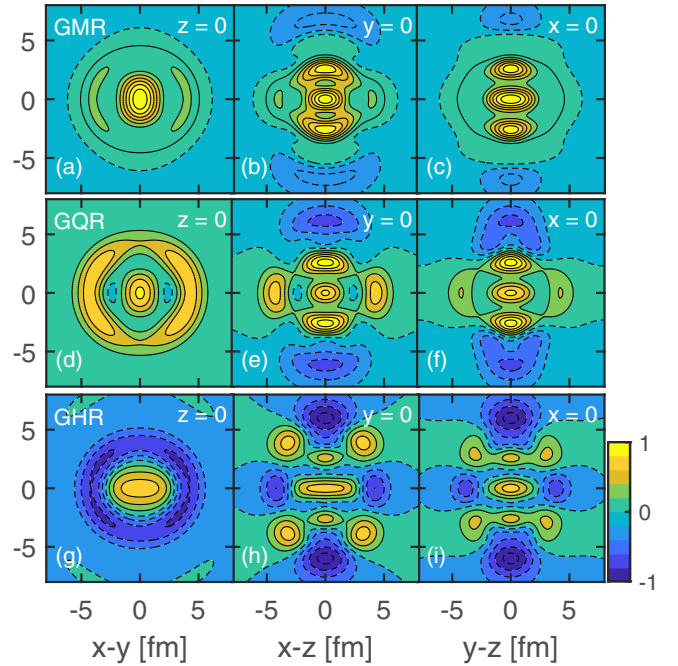


FIG. 5. Normalized transition densities at 11.5 MeV in ^{86}Ge for the resonance peaks of ISGMR [(a)–(c)], ISGQR with $K = 0$ [(d)–(f)], and ISGHR with $K = 0$ [(g)–(i)]. Contours with positive (negative) values are drawn with solid (dashed) lines.

the $E0$ - $E2$ - $E4$ coupling, and to check which vibration dominates, the microscopic structure of the triaxiality-induced resonance peak at 11.5 MeV is analyzed in the following. The distributions of the transition density on the $z = 0$, $y = 0$, and $x = 0$ planes are presented for ISGMR, ISGQR, and ISGHR in Fig. 5. Since ^{86}Ge is of a triaxial shape with $\gamma = 20.9^\circ$, the density distribution is stretched in the x direction and compressed in the y direction. Along the z axis, the phase of the transition density in the interior region is different from those spread outside. The transition densities show three nodes right next to each other in the interior region, which is a characteristic feature of hexadecupole vibrations. The three-node pattern is prominent in the transition densities of ISGMR, ISGQR, and ISGHR for the triaxiality-induced resonance peak, hence the contributions from hexadecupole vibrations are very strong and dominate. It should be noticed that, typically, for a quadrupole vibration, the phase of the transition density in the toroid on the $z = 0$ plane is opposite to that in the top (bottom) lobe along the z axis; but for a hexadecupole vibration, they have the same phase. Around the z axis, according to different phases, both constructive and destructive interference of the monopole, quadrupole, and hexadecupole vibrations can be identified for the triaxiality-induced peak in ^{86}Ge . For instance, the transition densities of ISGQR in panels (d)–(f) show significant mixture between quadrupole and hexadecupole vibrations, with both in-phase and out-of-phase vibrations between the peripheral region and the interior region on the $z = 0$ plane. The transition density of ISGMR in panels (a)–(c) is the result of the mixing of monopole, quadrupole, and hexadecupole vibrations.

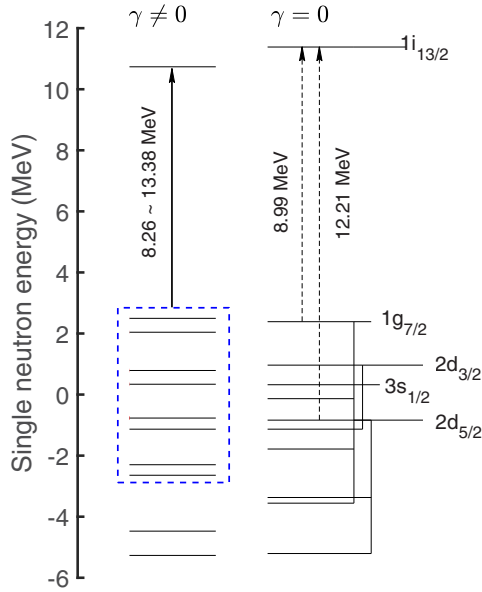


FIG. 6. Single neutron levels of ^{86}Ge ; the odd-parity orbits are omitted for simplicity. Particle-hole configurations with energy close to 10 MeV which are prohibited (dashed arrows) in the axial case may contribute (solid arrow) to $J = 4$ transitions in the triaxial case.

In weakly bound neutron-rich nuclei, there may be low-lying resonance peaks which are ascribed to the excitation of excess neutrons [45,56–58]. For ^{86}Ge , affected by the pairing correlations, the four neutrons outside the $N = 50$ magic core occupy the even-parity sdg shell. Since ISGMR has an even parity and involves $2\hbar\omega$ particle-hole transitions [1], in the deformed case the lowest available state a neutron in the sdg shell can be excited to is $1i_{13/2}$, which is an intruder state to the pfh shell and thus has a desired even parity. In principle, $J = 4$ transitions can be obtained through particle-hole configuration $2d_{5/2} \rightarrow 1i_{13/2}$, and $1g_{7/2} \rightarrow 1i_{13/2}$, etc. In the axially deformed case, the single-particle level with the angular momentum j splits into $(2j + 1)/2$ twofold degenerate orbits; those with larger absolute values of angular momentum projection Ω locate higher in energy when a nucleus is elongated. As illustrated in Fig. 6, though the particle-hole (ph) configurations $2d_{5/2} (\Omega_h = 5/2) \rightarrow 1i_{13/2} (\Omega_p = 1/2)$ and $1g_{7/2} (\Omega_h = 7/2) \rightarrow 1i_{13/2} (\Omega_p = 1/2)$ have energies close to 11.5 MeV (which are 12.21 and 8.99 MeV, respectively), the transitions are forbidden by the selection rule $\Omega_p - \Omega_h = K = 0$. In the triaxially deformed case, the projection of the angular momentum K of a nucleus is not a good quantum number. The aforementioned ph configurations are no longer hindered, which will contribute a $J = 4$ component to the resonance peak near 11.5 MeV.

Indeed, the $J = 4$ component of the vibration itself might be too weak to give noticeable effects alone. However, for the nucleus ^{86}Ge , affected by the particle-hole configurations provided by the triaxiality, the hexadecupole vibrations interplay with monopole and quadrupole vibrations dramatically, and eventually lead to a strong $E0$ - $E2$ - $E4$ coupling where hexadecupole vibration plays a dominate role.

IV. CONCLUSIONS

The isoscalar giant resonances for the triaxially deformed nucleus ^{86}Ge are studied with the quasiparticle finite amplitude method based on the covariant density functional DD-ME2 and a separable pairing force. The ISGMR for ^{86}Ge splits into three components when the triaxial deformation is considered. The deformation-induced double-peak structure for the ISGMR is clearly manifested when triaxiality is considered, so that the well-known monopole-quadrupole coupling is still valid for the triaxially deformed nucleus. In addition, a small resonance peak appears at $\omega \approx 11.5$ MeV in the strength functions of the ISGMR when the triaxiality is taken into account. The absence of similar phenomena in ^{64}Ge and ^{74}Ge shows that the triaxiality-induced low-lying monopole resonance peak may be significant only in neutron-rich nuclei. For ^{86}Ge , the triaxiality-induced resonance peak also appears at the same energy in the strength functions of ISGQR and ISGHR, implying the coupling among monopole, quadrupole, and hexadecupole vibrations. Evidence for the monopole-quadrupole-hexadecupole coupling is found by analyzing the spatial distribution of the transition density. The contribution from hexadecupole vibration is enhanced by the triaxiality. The emergence of the resonance peak at 11.5 MeV in the neutron-rich ^{86}Ge is a peculiar effect induced by the triaxiality. Therefore, it could serve as a fingerprint to identify the triaxiality of ^{86}Ge in future experiments.

ACKNOWLEDGMENTS

This work is partly supported by the National Key Research and Development Program of China (Grants No. 2018YFA0404400 and No. 2017YFE0116700), the National Natural Science Foundation of China (Grants No. 11621131001, No. 11875075, No. 11935003, and No. 11975031), the State Key Laboratory of Nuclear Physics and Technology, Peking University (Grant No. NPT2020ZZ01), and the China Postdoctoral Science Foundation under Grant No. 2020M680182. This work is supported by High performance Computing Platform of Peking University.

[1] M. N. Harakeh and A. van der Woude, *Giant Resonances: Fundamental High-Frequency Modes of Nuclear Excitation*, Oxford Studies in Nuclear Physics (Oxford University Press, Oxford, 2001).

[2] E. Lipparini and S. Stringari, *Phys. Rep.* **175**, 103 (1989).

[3] J. Blaizot, *Phys. Rep.* **64**, 171 (1980).

[4] T. Li, U. Garg, Y. Liu, R. Marks, B. K. Nayak, P. V. Madhusudhana Rao, M. Fujiwara, H. Hashimoto, K. Kawase,

- K. Nakanishi, S. Okumura, M. Yosoi, M. Itoh, M. Ichikawa, R. Matsuo, T. Terazono, M. Uchida, T. Kawabata, H. Akimune, Y. Iwao *et al.*, *Phys. Rev. Lett.* **99**, 162503 (2007).
- [5] N. V. Giai and H. Sagawa, *Nucl. Phys. A* **371**, 1 (1981).
- [6] D. H. Youngblood, H. L. Clark, and Y.-W. Lui, *Phys. Rev. Lett.* **82**, 691 (1999).
- [7] U. Garg and G. Colò, *Prog. Part. Nucl. Phys.* **101**, 55 (2018).
- [8] L. Trippa, G. Colò, and E. Vigezzi, *Phys. Rev. C* **77**, 061304(R) (2008).
- [9] L.-G. Cao, X. Roca-Maza, G. Colò, and H. Sagawa, *Phys. Rev. C* **92**, 034308 (2015).
- [10] X. Roca-Maza, M. Brenna, B. K. Agrawal, P. F. Bortignon, G. Colò, L.-G. Cao, N. Paar, and D. Vretenar, *Phys. Rev. C* **87**, 034301 (2013).
- [11] A. Klimkiewicz, N. Paar, P. Adrich, M. Fallot, K. Boretzky, T. Aumann, D. Cortina-Gil, U. Datta Pramanik, T. W. Elze, H. Emling, H. Geissel, M. Hellström, K. L. Jones, J. V. Kratz, R. Kulesa, C. Nociforo, R. Palit, H. Simon, G. Surówka, K. Sümmerer, and W. Waluś (LAND Collaboration), *Phys. Rev. C* **76**, 051603(R) (2007).
- [12] A. Carbone, G. Colò, A. Bracco, L.-G. Cao, P. F. Bortignon, F. Camera, and O. Wieland, *Phys. Rev. C* **81**, 041301(R) (2010).
- [13] T. Inakura, T. Nakatsukasa, and K. Yabana, *Phys. Rev. C* **84**, 021302(R) (2011).
- [14] X.-W. Sun, J. Chen, and D.-H. Lu, *Chin. Phys. C* **42**, 014101 (2018).
- [15] Y. Gupta, U. Garg, J. Matta, D. Patel, T. Peach, J. Hoffman, K. Yoshida, M. Itoh, M. Fujiwara, K. Hara, H. Hashimoto, K. Nakanishi, M. Yosoi, H. Sakaguchi, S. Terashima, S. Kishi, T. Murakami, M. Uchida, Y. Yasuda, H. Akimune *et al.*, *Phys. Lett. B* **748**, 343 (2015).
- [16] M. Itoh, H. Sakaguchi, M. Uchida, T. Ishikawa, T. Kawabata, T. Murakami, H. Takeda, T. Taki, S. Terashima, N. Tsukahara, Y. Yasuda, M. Yosoi, U. Garg, M. Hedden, B. Kharraja, M. Koss, B. Nayak, S. Zhu, H. Fujimura, M. Fujiwara *et al.*, *Phys. Lett. B* **549**, 58 (2002).
- [17] T. Peach, U. Garg, Y. K. Gupta, J. Hoffman, J. T. Matta, D. Patel, P. V. Madhusudhana Rao, K. Yoshida, M. Itoh, M. Fujiwara, K. Hara, H. Hashimoto, K. Nakanishi, M. Yosoi, H. Sakaguchi, S. Terashima, S. Kishi, T. Murakami, M. Uchida, Y. Yasuda *et al.*, *Phys. Rev. C* **93**, 064325 (2016).
- [18] M. N. Harakeh, K. van der Borg, T. Ishimatsu, H. P. Morsch, A. van der Woude, and F. E. Bertrand, *Phys. Rev. Lett.* **38**, 676 (1977).
- [19] U. Garg, P. Bogucki, J. D. Bronson, Y. W. Lui, C. M. Rozsa, and D. H. Youngblood, *Phys. Rev. Lett.* **45**, 1670 (1980).
- [20] U. Garg, P. Bogucki, J. D. Bronson, Y.-W. Lui, and D. H. Youngblood, *Phys. Rev. C* **29**, 93 (1984).
- [21] D. H. Youngblood, Y.-W. Lui, and H. L. Clark, *Phys. Rev. C* **60**, 067302 (1999).
- [22] M. Buenerd, D. Lebrun, P. Martin, P. de Saintignon, and C. Perrin, *Phys. Rev. Lett.* **45**, 1667 (1980).
- [23] S. Brandenburg, R. De Leo, A. G. Drentje, M. N. Harakeh, H. Janszen, and A. van der Woude, *Phys. Rev. Lett.* **49**, 1687 (1982).
- [24] Y. Abgrall, B. Morand, E. Caurier, and B. Grammaticos, *Nucl. Phys. A* **346**, 431 (1980).
- [25] S. Jang, *Nucl. Phys. A* **401**, 303 (1983).
- [26] S. Nishizaki and K. Andō, *Prog. Theor. Phys.* **73**, 889 (1985).
- [27] T. Nikšić, N. Kralj, T. Tutiš, D. Vretenar, and P. Ring, *Phys. Rev. C* **88**, 044327 (2013).
- [28] J. Kvasil, V. O. Nesterenko, A. Repko, W. Kleinig, and P.-G. Reinhard, *Phys. Rev. C* **94**, 064302 (2016).
- [29] G. Colò, D. Gambacurta, W. Kleinig, J. Kvasil, V. O. Nesterenko, and A. Pastore, *Phys. Lett. B* **811**, 135940 (2020).
- [30] S. Frauendorf and Jie Meng, *Nucl. Phys. A* **617**, 131 (1997).
- [31] K. Starosta, T. Koike, C. J. Chiara, D. B. Fossan, D. R. LaFosse, A. A. Hecht, C. W. Beausang, M. A. Caprio, J. R. Cooper, R. Krücken, J. R. Novak, N. V. Zamfir, K. E. Zyranski, D. J. Hartley, D. L. Balabanski, J.-y. Zhang, S. Frauendorf, and V. I. Dimitrov, *Phys. Rev. Lett.* **86**, 971 (2001).
- [32] S. W. Ødegård, G. B. Hagemann, D. R. Jensen, M. Bergström, B. Herskind, G. Sletten, S. Törmänen, J. N. Wilson, P. O. Tjøm, I. Hamamoto, K. Spohr, H. Hübel, A. Gørgen, G. Schönwasser, A. Bracco, S. Leoni, A. Maj, C. M. Petrache, P. Bednarczyk, and D. Curien, *Phys. Rev. Lett.* **86**, 5866 (2001).
- [33] X. Sun, J. Chen, and D. Lu, *Phys. Rev. C* **100**, 054605 (2019).
- [34] P. Ring and P. Schuck, *The Nuclear Many-Body Problem* (Springer, Berlin, 2004).
- [35] T. Nikšić, D. Vretenar, and P. Ring, *Prog. Part. Nucl. Phys.* **66**, 519 (2011).
- [36] J. Meng, *Relativistic Density Functional for Nuclear Structure* (World Scientific, Singapore, 2016).
- [37] J. Stone and P.-G. Reinhard, *Prog. Part. Nucl. Phys.* **58**, 587 (2007).
- [38] X. Sun, J. Chen, and D. Lu, *Phys. Rev. C* **99**, 054604 (2019).
- [39] Y. K. Gupta, U. Garg, J. Hoffman, J. Matta, P. V. Madhusudhana Rao, D. Patel, T. Peach, K. Yoshida, M. Itoh, M. Fujiwara, K. Hara, H. Hashimoto, K. Nakanishi, M. Yosoi, H. Sakaguchi, S. Terashima, S. Kishi, T. Murakami, M. Uchida, Y. Yasuda *et al.*, *Phys. Rev. C* **93**, 044324 (2016).
- [40] X. Sun, J. Chen, and D. Lu, *Phys. Rev. C* **98**, 024607 (2018).
- [41] T. Nakatsukasa, T. Inakura, and K. Yabana, *Phys. Rev. C* **76**, 024318 (2007).
- [42] H. Liang, T. Nakatsukasa, Z. Niu, and J. Meng, *Phys. Rev. C* **87**, 054310 (2013).
- [43] X. Sun and D. Lu, *Phys. Rev. C* **96**, 024614 (2017).
- [44] A. Bjelčić and T. Nikšić, *Comput. Phys. Commun.* **253**, 107184 (2020).
- [45] X. Sun, *Phys. Rev. C* **103**, 044603 (2021).
- [46] T. Inakura, T. Nakatsukasa, and K. Yabana, *Phys. Rev. C* **80**, 044301 (2009).
- [47] P. Avogadro and T. Nakatsukasa, *Phys. Rev. C* **84**, 014314 (2011).
- [48] M. T. Mustonen, T. Shafer, Z. Zenginerler, and J. Engel, *Phys. Rev. C* **90**, 024308 (2014).
- [49] M. Kortelainen, N. Hinohara, and W. Nazarewicz, *Phys. Rev. C* **92**, 051302(R) (2015).
- [50] K. Washiyama and T. Nakatsukasa, *Phys. Rev. C* **96**, 041304(R) (2017).
- [51] G. A. Lalazissis, T. Nikšić, D. Vretenar, and P. Ring, *Phys. Rev. C* **71**, 024312 (2005).
- [52] J. G. Valatin, *Phys. Rev.* **122**, 1012 (1961).
- [53] T. Nikšić, N. Paar, D. Vretenar, and P. Ring, *Comput. Phys. Commun.* **185**, 1808 (2014).
- [54] Y. Tian, Z. Ma, and P. Ring, *Phys. Lett. B* **676**, 44 (2009).
- [55] A. Negret and B. Singh, *Nucl. Data Sheets* **124**, 1 (2015).
- [56] J. C. Pei, M. Kortelainen, Y. N. Zhang, and F. R. Xu, *Phys. Rev. C* **90**, 051304(R) (2014).
- [57] N. Timofeyuk, D. Baye, and P. Descouvemont, *Nucl. Phys. A* **551**, 1 (1993).
- [58] X. Sun and J. Meng, *Phys. Rev. C* **105**, 044312 (2022).